Available online at www.sciencedirect.com
SCIENCE DIRECT®
Wear 255 (2003) 751–757
WEAR
www.elsevier.com/locate/wear

Communication

On the mechanisms of abrasive wear of polyamide fibres

J. Cayer-Barrioz [a,*], D. Mazuyer [a], P. Kapsa [a], A. Chateauminois [b], F. Bouquerel [c]

[a] *Laboratoire de Tribologie et de Dynamique des Systèmes, UMR 5513, CNRS, Ecole Centrale de Lyon, 36 avenue Guy de Collongue, 69130 Ecully, France*
[b] *Laboratoire de Physico-Chimie Structurale et Macromoléculaire, ESPCI, UMR 7615, 10 rue Vauquelin, 75231 Paris, France*
[c] *Rhodia Technical Fibres, BP 31, 69191 Saint-Fons Cedex, France*

Abstract

The abrasion resistance of fibres is a basic property in the textile industry since the fibres can be damaged during the manufacturing process. To understand the fundamental mechanisms of abrasion of 40 μm diameter polyamide fibres, a tribometer using a fibre-cylinder contact configuration immersed in water has been developed. This instrumented device controls tribological parameters such as the sliding speed, the environment and the tension applied to the fibre. A reference experimental procedure has been defined in order to run comparative experiments where the former parameters were varied. The number of rod revolutions leading to the fibre rupture has been selected as a macroscopic wear criterion. It is found to be independent of the sliding speed, in the investigated range of velocities. A simple thermal analysis of the sliding contact confirms that the contact heating is limited by the cooling effect of water. Microscope observations of worn fibres reveal abrasive scars and defibrillations on the fibre surface and are used to characterize the wear kinetic. From these observations, it is shown that the abrasive process is responsible for a continuous diminution of the fibre cross-section until the creep failure stress is achieved locally.

Keywords: Abrasive wear; Polyamide fibre; Scratch

1. Introduction

The most effective applications of polymers as engineering materials often require a better understanding and control of their surface mechanical properties. This is particularly relevant in the polymer fibre industry. The fibre forming process controls the structure and the mechanical and thermal properties of the fibre [1]. Two models have been developed to present the microfibrillar morphological structure of polyamide fibres: Prevorsek has proposed a microfibrillar "swiss-cheese" model when Peterlin has preferred a two phase microfibrillar model [2]. It has been shown that both models are suitable for polyamide fibres, depending on the forming process. The fibre structure strongly influences its tribological behaviour. Moreover, the mechanical properties of hydrophilic polymers such as polyamides are dependent on the presence of water in the environment [3]. The decrease in the mechanical properties of polyamide fibres is due to the diffusion of water molecules into the amorphous regions of the semi-crystalline polymer leading to plasticisation and the rupture of intermolecular hydrogen bonds [4]. The tribological behaviour of polyamide is also dependent on the presence of water. Therefore, the environment has to be controlled.

During the manufacturing process, the fibres undergo a wide range of mechanical stresses under which their surface may present damage caused by abrasion. Such damage shorten the fibre life. Consequently, the abrasion resistance is a fundamental property of polymers. The scratching method is convenient to characterize polymer abrasion resistance since it reproduces a number of contact conditions encountered in practice [5]. In previous studies, scratching maps for a single asperity contact have been built [5,6]. Surface scratch deformation mechanisms that occur during the contact have been described for various strain rates, applied normal loads and indenter geometries. However, these maps do not provide all the necessary data about the damage mechanisms, especially for polyamide fibres, or severity under all conditions [5]: the strain rates and loads are indeed much lower than the ones used in the fibre industry. Moreover, the scratching method does not allow us to study the abrasive wear of fibres from a macroscopic point of view.

The purpose of this study is to contribute to the understanding of the abrasive wear mechanisms of polyamide fibres and to identify the microscopic and macroscopic relevant parameters in the abrasive wear process. In order to identify the tribological parameters determining the fibre abrasion resistance, a test simulating the fibre abrasion has

* Corresponding author. Tel.: +33-472-186-288; fax: +33-478-433-383.
E-mail address: juliette.cayer-barrioz@ec-lyon.fr (J. Cayer-Barrioz).

0043-1648/03/$ – see front matter © 2003 Elsevier Science B.V. All rights reserved.
doi:10.1016/S0043-1648(03)00176-5

been developed in which tribological parameters such as speed, environment and applied tension are controlled. A reference experimental procedure has been defined in order to run comparative experiments by varying test parameters.

2. Experimental details

2.1. The abrasion test

The fibre abrasion process is induced using a tribometer which realises a contact between a fixed tight fibre and a rotating "abrasive" rod, as shown in Fig. 1. Fifteen fibres can be simultaneously tested in each experiment. A statistical analysis of the fibre rupture can then be made. The chosen abrasion resistance criterion is the average time to rupture of the 15 tested fibres.

A dead weight and pulley system is used to produce a tension, F_1, on the free end of the fibre. The tension on the other extremity F_2 is measured by a force transducer, which has a maximum load capacity of 0.2 N. It may be assumed that the diameter of the fibre ($\Phi = 40\,\mu$m) is small compared to that of the rod. In our experiment, the total angle of contact between the fibre and the rod is $\alpha = \pi/2$. A friction coefficient μ between the fibre and the rod may be calculated along the contact by the following relation [7,8]:

$$F_2 = F_1 e^{\alpha\mu} \quad (1)$$

For a given applied load F_1, the measured friction coefficient varies with both the tensile load caused by the rotation of the rod and the number of fibre wraps around the rod. The elongation of one fibre out of 15 is measured during the experiment via a displacement sensor. A maximum elongation of 20 mm can be detected.

Three parameters can be accurately controlled in the tribometer:

- The environment: the rod and fibres are immersed in a controlled temperature bath of mineral water in order to reduce the effects of variable moisture on polyamide. The bath temperature is maintained at $25 \pm 1\,^{\circ}$C. A simple calculation of minimum film thickness h_0 in the contact by applying Moes-Venner EHL theory [9] for water as lubricant provides a h_0 of about 1 Å which is 1000 lower than the rod roughness. This shows that water is unable to generate a lubricating film.
- The abrasive rod surface roughness: the roughness R_a of the 10 mm diameter rod is 1.6 μm. The rod asperities have a conical shape. The mean distance peak-valley is 13 μm. The rod rotation speed can reach 3000 rpm, which corresponds to a linear speed of 1.5 m/s. The rod is made of steel covered by a hard ceramic coating.

  Topographic measurements have been performed on the rod using a WYKO® optical interferometer before and after the wear test. No significant change in the rod surface roughness is noticed which suggests that experiments do not cause rod wear, and that the test corresponds to the wear of the fibres only.
- The applied load: it varies from 2 to 7 g.

The fibres are made of thermoplastic semi-crystalline polyamide 6 and have a "swiss-cheese" structure. Their round section has a mean diameter of 40 μm. Molecular mass M_n is about 26,000 g/mol. These fibres have been drawn at 300% and their rupture stress is 0.7 GPa for true rupture strain of 50% [10] when water saturated.

2.2. Experimental procedure

The test conditions have been chosen to optimize repeatability while remaining within the capabilities of the apparatus. Therefore, a reference experimental procedure has been defined: the initial applied tensile stress of 22 MPa is produced by a 3-g dead weight and the rod rotation speed is

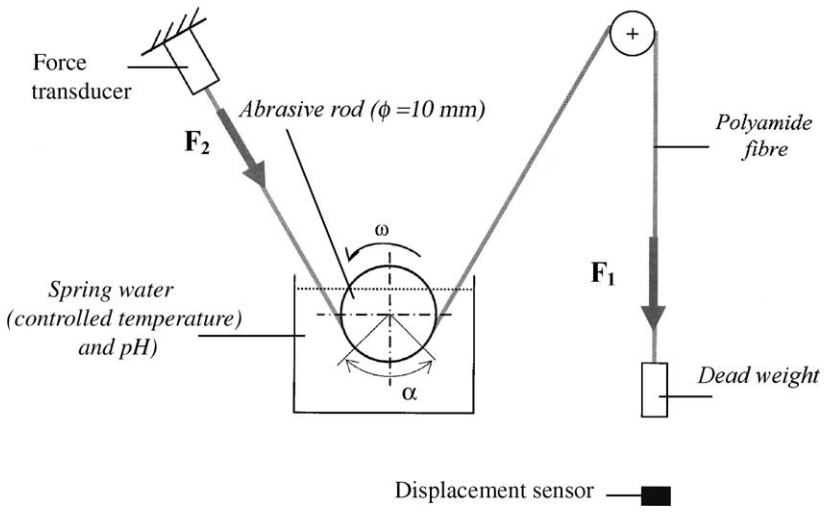

Fig. 1. Schematic of the tribometer. A rotating abrasive rod rubs a fixed tight fibre loaded using a dead weight. The contact is fully immersed in water. A force transducer measures the friction induced tension, F_2. The fibre elongation is simultaneously monitored using a displacement sensor.

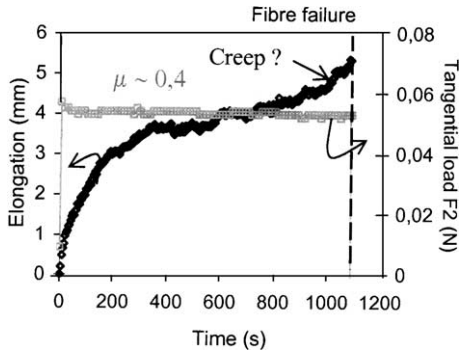

Fig. 2. Evolution of the tension force F_2 (□) and the fibre elongation (◇) during the experiment. Reference tests were performed at $v = 300$ rpm, at 25 °C and for a dead weight of 3 g. The measured force F_2 remains constant and corresponds to an apparent friction coefficient of 0.4. The fibre steadily lengthens with time to reach 5 mm at the failure which occurs within 18 min.

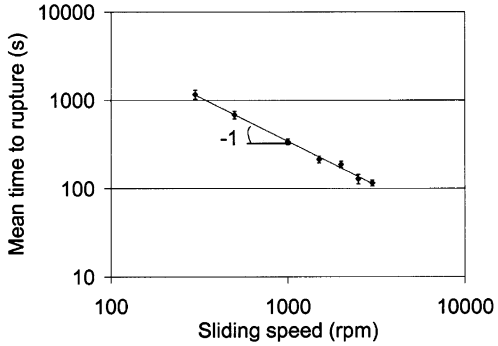

Fig. 3. Influence of the sliding speed on the mean time to fibre failure. The curve puts forward that the fibre failure is independent of the rod sliding velocity and always occurs for a rod revolution number of 5600 or a sliding distance of 176 m.

300 rpm which corresponds to a linear speed at the contact of 0.15 m/s. Fibres are immersed in spring water 24 h before testing. If not specified, all presented tests were performed at reference conditions.

Within these conditions, the evolution of the friction force caused by the rod rotation and the fibre elongation is measured versus time. Typical evolutions of these parameters are shown in Fig. 2. The apparent friction coefficient between the fibre and the rod is calculated from the relation (1). It remains constant at 0.4 during the experiment and it sharply decreases at the fibre rupture. The fibre elongation increases continuously to reach 5 mm at the fibre rupture which occurs within 18 min.

3. Results

3.1. Effects of the sliding speed

Test have been carried out at different rod velocities between 300 and 3000 rpm. The measured friction coefficient remains unchanged within this speed range. The evolution of the average time to failure versus the rod speed in a logarithmic scale (Fig. 3) shows that the average time to rupture is inversely proportional to the rod velocity. Therefore, a macroscopic wear criterion is defined as the number of rod revolutions (or the rod sliding distance) leading to the fibre failure. This parameter is approximately 5600 (or 176 m) in spite of the changes in the sliding velocity. This also tends to demonstrate that thermal effects can be neglected in the studied velocity range due to the cooling capability of the water. A very low glass transition temperature for water saturated fibre (−15 °C) [11] might explain that the sliding distance leading to the fibre failure is independent of the sliding velocity within the speed range (0.1–1.6 m/s) since the polymer is in the rubbery state.

3.2. Fibre wear processes

The damaged fibres have been observed in SEM and AFM before the rupture occurs. A macroscopic analysis of the contact deformation modes is made possible thanks to SEM observations. In the contact zone which is 8 mm long, every fibre presents the same abrasive scratches aligned along the sliding direction as shown in Fig. 4a. The scratch size leads us to use AFM imaging to characterise the worn fibres locally (Fig. 4b). The abrasive scratches are about 3 μm wide and 0.5 μm deep. Since the mean diameter of microfibrils is about 10 nm [12], these scratches confirm an abrasive wear mechanism of the fibre and reveal the presence of plastic deformation at the fibre surface.

The fibre cross-section decreases progressively from the centre of the contact zone until the failure point, in the neighbourhood of which, the fibre is completely flattened (Fig. 5). Defibrillations are also observed along the fibre edges. Worn fibre cross-section measurements are used to quantify the material loss.

3.3. Wear kinetic

Experiments have been carried out for a dead weight of 3 and 5 g. These tests have been stopped after different sliding distances in order to characterise the wear kinetic and to observe the evolution of the fibre damages along the contact zone. The fibre is not worn homogeneously along the contact zone. The schematic evolution of the fibre profile along the contact is shown in Fig. 6 for a sliding distance of 47 m. The most damaged part of the fibre is located at 0.5 mm (respectively 2.4 mm) from the entrance (F_2 edge) of the contact at 3 g (at 5 g). The worn fibre cross-section at that point is estimated from SEM observations (Fig. 7). Its evolution is plotted versus the sliding distance in Fig. 8. Both curve profiles show the same tendency: first an increase in the worn cross-section followed by a plateau and then a rise. The plateau corresponds to a 50% rate of cross-section wear. Schematic shape of the fibre cross-section is drawn

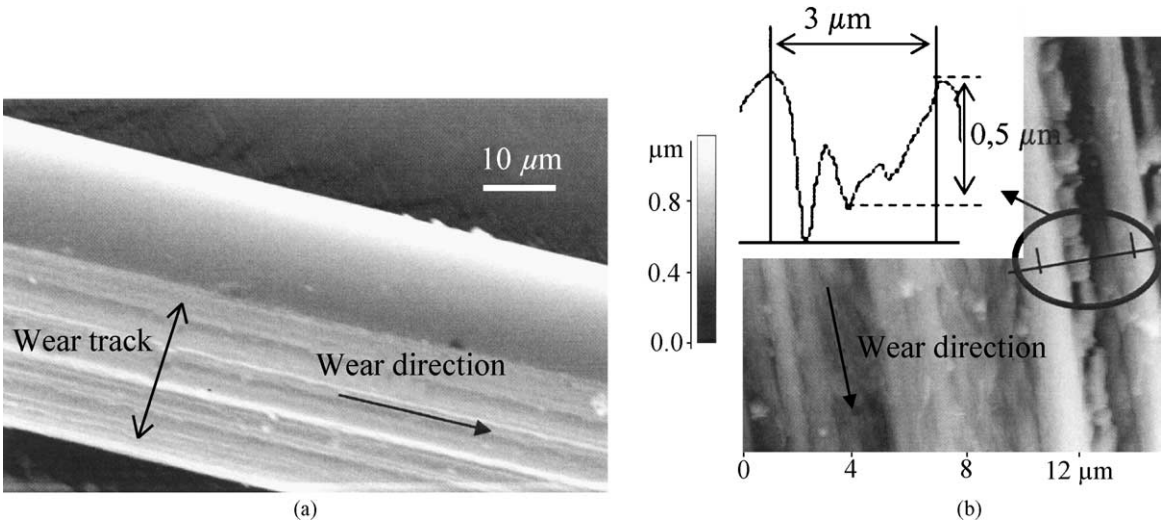

Fig. 4. (a) SEM, and (b) AFM observations of damaged fibres in the contact zone and scratch profile before the occurrence of fibre failure (a sliding distance of 47 m). Continuous abrasive scratches are oriented along the sliding direction. These observations also reveal plastic deformation at the fibre surface.

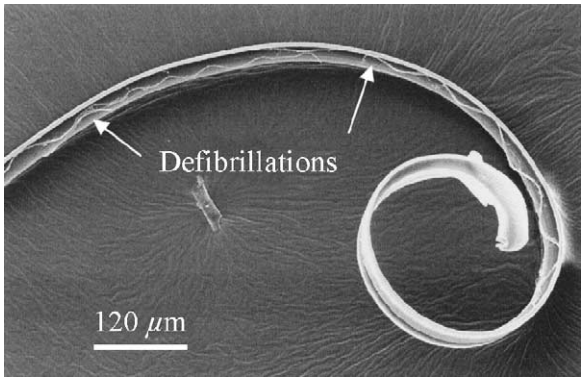

Fig. 5. SEM observations of a damaged fibre after failure. The fibre cross-section diminishes along the contact zone. Close to the rupture point, the fibre is completely flattened. Defibrillations are shown along the fibre sides.

in Figs. 7 and 8. For the early first steps of the wear process (first 16 m), the cross-section remains circular (Fig. 7a). Then the fibre is progressively flattened until the fibre worn cross-section reaches 50% (Fig. 7b) of its initial area. In the last steps, the fibre eventually forms a ribbon (Fig. 7c). The comparison of worn cross-section measured at different applied tensions reveals an acceleration of the wear kinetic with increasing applied tension.

From assessment of the worn fibre profile as a function of the rod sliding distance (an example is presented in Fig. 6), a wear volume can be estimated. Fig. 9 shows the evolution of this wear volume versus the rod sliding distance for tests performed using a dead weight of 3 and 5 g. Both plots increase linearly with the sliding distance. The measurement accuracy does not allow to show significant differences between the wear volumes in both cases. Wear rates W_s can be calculated from:

$$W_s = \frac{\text{Wear volume}}{\text{Load} \times \text{sliding distance}} \quad (2)$$

It is found that 1.2×10^6 μm^3/N m is obtained for 3 g and 2.0×10^6 μm^3/N m for 5 g. It confirms that the wear kinetic is accelerated with increasing applied tension.

4. Discussion

4.1. Mechanical and thermal analysis of the contact

From the Hertzian theory, an interfacial contact shear stress can be estimated. It is assumed that the radius of the rod (R) is infinitely large compared to that of the fibre (r). Therefore, the contact geometry between the fibre and the rod can be approximated by the general case of a long

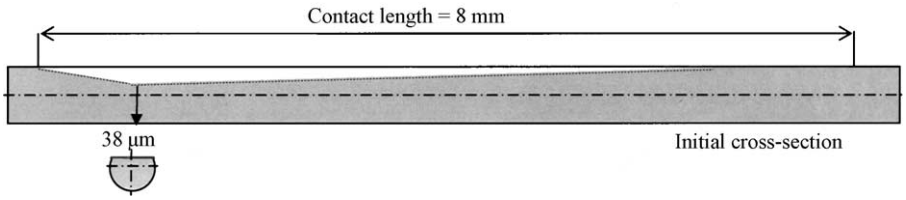

Fig. 6. Schematic profile of the fibre along the contact for a sliding distance of 47 m. The fibre shows uneven shape along the contact.

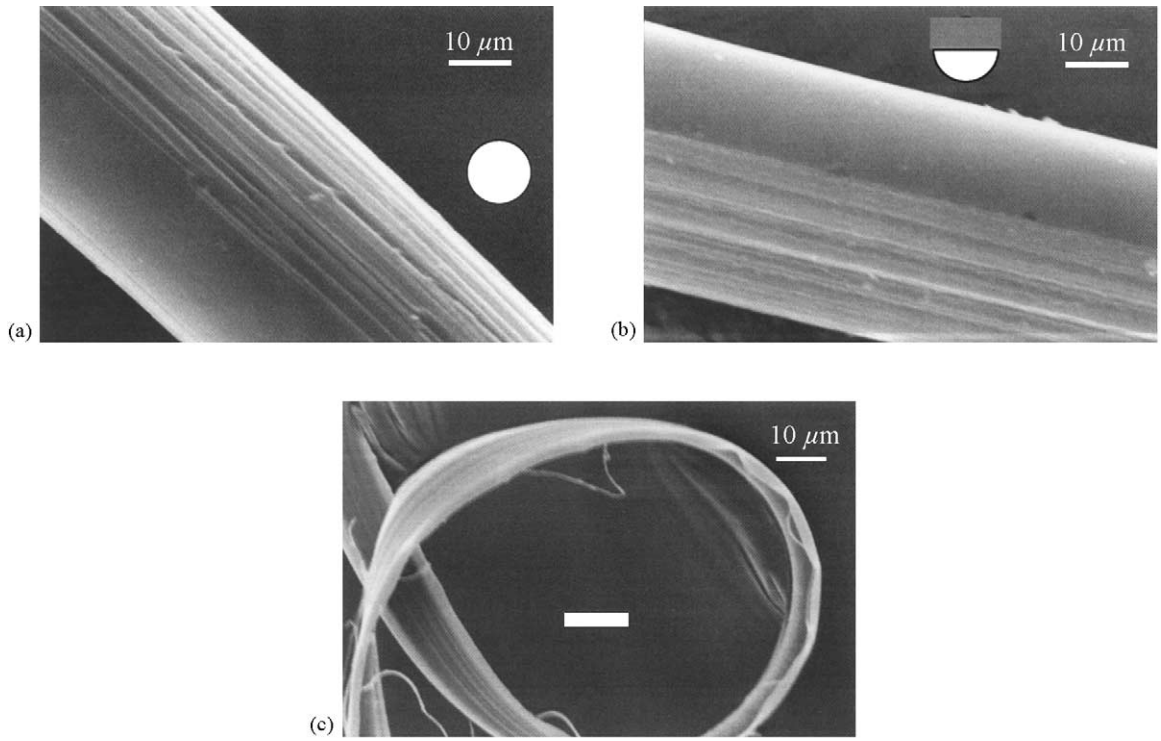

Fig. 7. SEM observations of damaged fibres at different sliding distances (a) 16 m for a dead weight of 3 g: the fibre still presents circular cross-section; (b) 47 m for a dead weight of 3 g: the fibre is progressively flattened; (c) 110 m for a dead weight of 3 g: the fibre forms a ribbon. The schematic shape of the fibre cross-section is drawn.

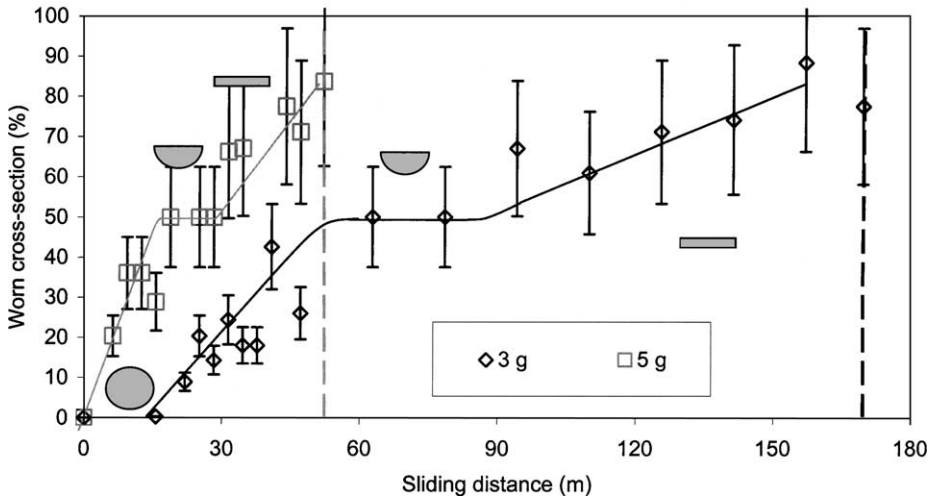

Fig. 8. Changes in the worn fibre cross-section at the most damaged point of the fibre as a function of the sliding distance. Experiments have been carried out at 3 g (◇) and 5 g (□). The schematic shape of the fibre cross-section at the various abrasion stages is drawn.

cylinder pressing against a flat [8]. The mean Hertzian contact pressure (P_{mean}) along the contact between the fibre and the rod is given by:

$$P_{mean} = 0.625\sqrt{\frac{LE'}{2r}} = 0.625\sqrt{\frac{F_1 E' e^{\alpha\mu}}{2Rr}} \quad (3)$$

where E' is the reduced Young's modulus of elasticity and L is the contact load per unit length of fibre. The apparent mean contact pressure is about 3 MPa. The polyamide plastic yield stress, $Y_{polyamide}$, is about 70 MPa:

$$P_{mean} = 3\,\text{MPa} < 1.1 \times Y_{polyamide} = 80\,\text{MPa} \quad (4)$$

Therefore, the macroscopic contact is elastic. However, SEM and AFM observations show plastic deformation (Fig. 4). Consequently, the rod roughness which governs the real contact pressure is a key parameter in the damage process.

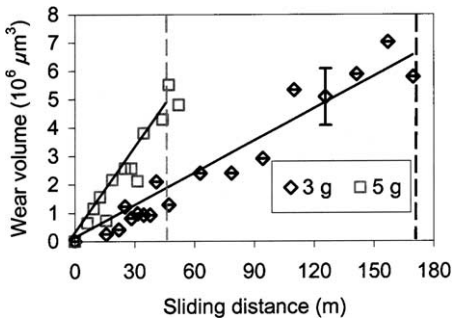

Fig. 9. Determination of the wear volume as a function of the sliding distance. Experiments have been carried out at 3 g (◇) and 5 g (□). No significant differences between the wear volumes in both cases can be shown, due to the measurement inaccuracy.

The literature emphasises the importance of thermal effect role in the contact, especially for polymers. Distribution of the heat generated in the contact during each rod revolution by the friction process and the contact heating ΔT are estimated by applying the laws of energy conservation and heat transfer [13]. For our conditions, it is found that 98% of the heat generated by friction is dissipated into the rod. The temperature profile [14] in the contact decreases as a function of time:

$$T(t) = T_{\text{solid}} + (T_{\text{interface}} - T_{\text{solid}})\mathrm{e}^{-t/\tau_{\text{cooling}}} \quad (5)$$

where a cooling time τ_{cooling} has been introduced. It represents the time required to cool the heating source down and is given by:

$$\tau_{\text{cooling}} = \frac{MC_{\text{p}}}{\alpha_{\text{e}} S} \quad (6)$$

where α_{e} depends on the environment, S is the apparent contact area and M is the mass to cool down. In a first macroscopic approach, the presence of water is not taken into account in these calculations. For an elastic contact, the contact heating calculated under the reference conditions is 1 °C/rod revolution and 2×10^{-4} s are required to cool the contact down in the air. The revolution time of the rod at this speed is 0.2 s, much superior than the cooling time. Consequently, the contact is cooled down and there should be no fibre heating. Dry (without water) experiments have been carried out at the same rod velocity and SEM observations clearly show melting of polyamide. This result is contradictory to the above theoretical analysis. Therefore, we can think that the heating is localised at the microasperity level.

The water film thickness shows that water is unable to generate a lubricating film which means that the rod asperities support most of the load in the contact. These findings confirm that the local contact conditions between the fibre and the microasperities are of primary importance regarding the heat generation at the polymer/steel contact interface. The asperity is assumed to be represented by a 1-μm radius sphere. For a local contact asperity-fibre, the contact heating reaches 15 °C/revolution. If the environment is taken into account, cooling down the contact requires either 5 s in air or 0.12 s in water (since τ_{cooling} depends on the environment) when the revolution time is still 0.2 s. The thermal analysis results are summarised in Table 1.

Table 1
Summary of the thermal analysis of the contact

	ΔT (°C)	τ_{cooling} [air] (s)	τ_{cooling} [water] (s)	Revolution period (s)
Elastic contact	1	2×10^{-4}	$<2 \times 10^{-4}$	0.2
Asperity-fibre contact	15	5	0.12	0.2

These results emphasize the role of the water in the contact.

This simple thermal analysis confirms that fibre heating is limited by the cooling effect of water since τ_{cooling} (air) = 5 s > revolution period = 0.2 s > τ_{cooling} (water) = 0.12 s. The presence of water influences the fibre mechanical properties and the wear mechanisms.

4.2. Failure mechanisms

During the abrasive process, fibres undergo creep, material loss and tensile stress. These coupled damage modes are responsible for the fibre failure.

Tensile tests on water saturated fibre give a true rupture strain (ε_{r}) of 50% and a true rupture stress (σ_{r}) of about 0.7 GPa. Static creep experiments have been carried out for a 3-g applied load (tensile stress ~22 MPa) on water saturated fibre during 40 min. In such conditions, the increase of length of a 50-cm long fibre is 0.8 mm which corresponds to a 0.1% strain. The fibre elongation ΔL measured during the abrasive experiment reaches 5 mm (Fig. 2) for a contact length of 8 mm, which corresponds roughly to a 50% strain. This calculation implies that only the portion of the fibre located within the contact is significantly lengthened during the experiment. The comparison of both strains suggests that creep under 22 MPa cannot explain by itself the occurrence of failure.

The measured strain during abrasive experiment corresponds to the one obtained by tensile tests. SEM observations provide the fibre cross-section S_{rupture} at the rupture point. Therefore, the rupture stress (σ_{r}) may be calculated at the rupture point from the apparent μ friction coefficient as following:

$$(\sigma_{\text{r}}) = \frac{F_1 \mathrm{e}^{\alpha\mu}}{S_{\text{rupture}}} \quad (7)$$

It gives a 400-MPa stress which is much lower than the rupture stress measured with tensile tests under water. Creep experiments have been carried out for a 50-g applied load on water saturated fibre. After rupture, the cross-section S_{m} is measured via SEM. The true applied stress ($F_1 \mathrm{e}^{\alpha\mu}/S_{\text{m}} \sim$ 400 MPa) leads to the fibre failure.

Therefore, it appears that the abrasion process promotes a continuous diminution of the fibre cross-section until the creep failure stress is locally reached. The elongation of the

fibre, and therefore the fibre failure, are due to wear activated creep in the contact region.

5. Conclusions

Our study focuses on the abrasion resistance of polyamide fibres. An abrasive rod-fibre tribometer has been developed in order to simulate the fibre abrasion under controlled conditions.

An experimental study of the wear of water immersed polyamide fibres at various velocities have revealed that the number of revolutions of the rod leading to the fibre rupture is independent of the rod speed. A simple thermal analysis confirms that the cooling capability of the water limits the thermal effects.

SEM and AFM observations have shown that damaged fibres reveal abrasive scratches and defibrillations on the fibre surface. The wear kinetic has been determined and shows that an increased load accelerates the wear process.

From these observations, some hypotheses on the wear mechanisms have been established. First, abrasion causes a diminution of the fibre cross-section until the creep failure stress is locally reached. A simple mechanical analysis shows the importance of the rod roughness. Second, the wear process causes the fibre elongation, which suggests that two frequencies have to be considered in the wear process: the rod sliding speed and the strain rate of the fibre associated to its elongation.

A macroscopic wear criterion is defined as the number of rod revolutions (or the sliding distance) leading to the fibre rupture and a relevant microscopic parameter is the rod roughness. The influence of the fibre structure is also a chief parameter which has not been studied yet.

Acknowledgements

This study is financially supported by Rhodia Technical Fibres. The authors wish to express their gratitude to G. Robert (Rhodia—Lyon Research Center), J.-C. Abry and G. Meille (Ecole Centrale Lyon) for helpful discussion and technical assistance.

References

[1] S. Mukhopadhyay, Polym. Eng. Sci. 34 (1994) 371–376.
[2] V. Bukosek, D.C. Prevorsek, Int. J. Polym. Mater. 47 (2000) 569–592.
[3] R.J. Hernandez, R. Gavara, J. Polym. Sci. Part B: Polym. Phys. 32 (1994) 2367–2374.
[4] G.W. Ehrenstein, F. Montagne, Matériaux polymères. Structure, propriétés et applications, Hermes Science Publications, Paris, 2000.
[5] B.J. Briscoe, P.D. Evans, E. Pelillo, S.K. Sinha, Wear 200 (1996) 137–147.
[6] B.J. Briscoe, E. Pelillo, S.K. Sinha, Polym. Eng. Sci. 36 (1996) 2996–3005.
[7] P. Bouré, Ph.D. Thesis, Ecole Centrale de Lyon, 1999, pp. 147–152.
[8] P.I. Lacey, S. Gunsel, Lubr. Eng. 57 (2001) 13–22.
[9] S. Hollinger, Ph.D. Thesis, Ecole Centrale de Lyon, 1999, pp. 2–25.
[10] M.F. Ashby, D.R.H. Jones, Matériaux. 1. Propriétés et applications, Bordas, Paris, 1991.
[11] Private communication with Rhodia Technical Fibers, 2000.
[12] D.C. Prevorsek, J. Macromol. Sci. Phys. B12 (4) (1976) 447–485.
[13] G.W. Stachowiak, A.W. Batchelor, Engineering Tribology, Butterworth-Heinemann, Woburn, 2001.
[14] Gregorik, Echangeurs de chaleur, Béranger, Paris, 1965.